



Journal of Geophysical Research: Atmospheres

RESEARCH ARTICLE

10.1029/2018JD028407

Key Points:

- The relationship between radii of two hydrometeors under different electric field for streamer initiation in the gap is documented
- The relationship between radii of two hydrometeors connected with a discharge channel for streamer initiation on outside periphery is provided
- For realistic hydrometeor size distributions the streamer initiation on outside periphery requires fields greater than or equal to 0.5E_k at altitudes 3 and 6 km

Correspondence to:

Q. Cai, qzc104@psu.edu

Citation:

Cai, Q., Jánský, J., & Pasko, V. P. (2018). Initiation of streamers due to hydrometeor collisions in thunderclouds. *Journal of Geophysical Research: Atmospheres*, 123, 7050–7064. https://doi.org/10.1029/2018JD028407

Received 29 JAN 2018
Accepted 30 MAY 2018
Accepted article online 20 JUN 2018
Published online 17 JUL 2018

Initiation of Streamers Due to Hydrometeor Collisions in Thunderclouds

Qiheng Cai¹, Jaroslav Jánský¹, and Victor P. Pasko¹

¹CSSL Laboratory, Department of Electric Engineering, School of Electrical Engineering and Computer Science, The Pennsylvania State University, University Park, PA, USA

Abstract In order to initiate streamers and leaders under thunderstorm conditions the electric field should reach values higher than the critical breakdown field E_k (i.e., $\sim 30 \text{ kV} \cdot \text{cm}^{-1} \cdot \text{atm}^{-1}$). However, the maximum electric field in thunderstorms measured by balloons is $\sim 6-9 \text{ kV} \cdot \text{cm}^{-1} \cdot \text{atm}^{-1}$. In present work, to achieve the electric field amplification required for streamer initiation, a system of two approaching spherical hydrometeors is investigated. Streamer initiation is determined from a Meek number, describing electron multiplication in fields above E_k . We have found the relationships between radii of particles for successful streamer initiation in the gap between these two particles and also on the outside periphery of the two particle system when the particles are connected by a discharge channel. Furthermore, we estimated the frequency of streamer initiation using three realistic hydrometeor size model distributions available in the literature and found that the scenario of streamer initiation on the outside periphery is only possible for relatively high electric fields $\geq 0.5E_k$ at altitudes of 3 and 6 km.

1. Introduction

The initiation of lightning leaders in low thundercloud fields remains one of the unsolved problems in lightning discharge physics (Dwyer & Uman, 2014, section 3, and references therein). One of the initial conditions required for the formation of a hot leader channel is initiation of nonthermal streamer discharges. Streamers can be initiated from electron avalanches; however, the problem of existence of an electric field strong enough for streamer initiation in thunderclouds remains, mainly because these fields are not observed on large scales in thunderstorms.

Marshall et al. (2005) reported the maximum electric field associated with lightning initiation in thunderstorms measured by balloon to be $3.7 \, \text{kV} \cdot \text{cm}^{-1} \cdot \text{atm}^{-1}$. Stolzenburg et al. (2007) reported later nine balloon soundings, which were adversely affected by lightning and therefore interpreted to be near lightning flash initiation. The largest observed field was $6.26 \, \text{kV} \cdot \text{cm}^{-1} \cdot \text{atm}^{-1}$, and the largest estimated field was $9.29 \, \text{kV} \cdot \text{cm}^{-1} \cdot \text{atm}^{-1}$ (altitudes in this sounding were estimated above 5.2 km, where the radiosonde data ended). Additional maximum electric field measurements are summarized in Dwyer and Uman (2014, Table 3.1, and references therein). All measured fields are smaller than the breakdown electric field E_k defined by the equality of ionization and two body attachment collision frequencies of electrons in air, which is $\simeq 28.7 \, \text{kV} \cdot \text{cm}^{-1} \cdot \text{atm}^{-1}$ (e.g., Morrow & Lowke, 1997).

One of the possible explanations for the streamer corona initiation is that hydrometeors, such as raindrop, hail and graupel greatly intensify the local electric field by at least an order of magnitude to initiate an electron avalanche. Liu, Kosar, et al. (2012) and Shi et al. (2016) showed that a positive streamer can be initiated from a hydrometeor modeled as an ionization column in a uniform applied field $0.5 E_k$. Sadighi et al. (2015) indicated that initiation of stable streamers from thundercloud hydrometeors in a $0.3 E_k$ electric field is possible and that the dimension of the model hydrometeor plays an important role in streamer initiation. Dubinova et al. (2015) indicated that at an altitude of 5.5 km, if elongated ice particles have length of 6 cm and there is an available electron density of 100 cm^{-3} , lightning can be initiated in low ambient electric field, which is 15% of the breakdown field E_k . Babich et al. (2016), by using a raindrop model, demonstrated that an electric field can be increased in the vicinity of a charged raindrop such that the electron avalanche to streamer transition is possible for raindrops with diameter of $\sim 0.5 - 1.5 \text{ mm}$ and with a net charge on the order

 $\ensuremath{\mathbb{G}}$ 2018. American Geophysical Union. All Rights Reserved.

of 100 to 400 pC. Babich et al. (2017) further studied the positive streamer formation around charged, needle-shaped ice hydrometeors and found that the external field value required for streamer initiation was higher than $8 \, \text{kV} \cdot \text{cm}^{-1} \cdot \text{atm}^{-1}$.

Particle pairs or chains create more favorable conditions for initiation of lightning discharge than a single precipitation particle in low electric fields (Nguyen & Michnowski, 1996). Blyth et al. (1998) indicated existence of a significant probability of corona initiation in a low local electric field, which is lower than 400 kV/m, by measuring the fraction of collisions resulting in the emission of detectable corona for three types of hydrometeor interactions (such as [1] warm drop pairs, [2] supercooled drop pairs, and [3] a supercooled drop and a graupel pellet). Mazur et al. (2015) employed an array of conducting particles to test its effect on the processes in the streamer-leader formation in lightning, concluding that an array of particles might behave as the equivalent of a single large, weakly conducting and charged body, which would have a total field enhancement factor significantly greater than that of an individual particle.

Cai et al. (2017) studied streamer initiation between two spherical particles with the same radii and numerically estimated related collision frequency in a thundercloud region with a relatively large volume of $2 \text{ km} \times 0.1 \text{ km} \times 0.8 \text{ km}$ and a relatively small volume of $10 \text{ m} \times 10 \text{ m} \times 10 \text{ m}$, respectively. It was shown that particles with radii of \sim 2.5 mm can initiate streamers in the minimum field required for propagation of positive streamers in air (i.e., \sim 4.4 kV/cm at ground level). The electric field created between two colliding particles is significantly enhanced, leading to formation of streamers. In order to participate in formation of leaders in large volumes around particles the streamers should find a pathway to escape from interparticle space. The authors suggested several scenarios of the streamer escape. Such scenario when the streamer is ignited on the outside of one of the spheres, following the discharge bridging gap between the spheres, was studied by Cooray et al. (1998). Cooray et al. (1998) studied particles with the same radii and found that the minimum field for streamer initiation should be high, on the order of \sim 2/3 E_R . In present work, we improve the previous studies by analyzing the two spherical particles with different radii for streamer ignitions both between and outside of the two particle system.

An important part of present work is usage of realistic models for distribution of hydrometeors with different dimensions inside of thunderclouds and evaluation of their collision frequencies. A considerable number of papers have been published concerning raindrop size distribution based on the early work by Marshall and Palmer (1948). Marshall and Palmer (1948) initially proposed the analytical formula for raindrop distribution with size which has the exponential form and is based on measurements of raindrops. Waldvogel (1974) used this analytical formula to describe the measured raindrop spectra. Atlas and Ludlam (1961) indicated that size spectrums of particles in a hailstorm could be represented by this exponential form as well. This form is also considered as a reference to verify the relationships between diameters of ice particles and their respective concentrations observed by Auer (1972) and Dye et al. (1986). Testud et al. (2001) further proposed a normalization method for raindrop spectra based on Marshall and Palmer (1948) for applications in cloud physics and cloud remote sensing.

2. Model Formulation

2.1. Electric Field of Two Separated Uncharged Spheres in a Uniform Electric Field

We use the image method based on Cloete and van der Merwe (1998) and Jackson (1999, p. 63) to get the solution for the electric field in the gap between two spheres placed in a uniform electric field. Dubinova et al. (2015) modeled lightning inception from large ice particles which behave as dielectrics instead of conductors and indicated that high relative permittivity 90 is responsible for field enhancement at the tip of ice particle. Additionally, due to very low field inside the ice hydrometeor, the hydrometeor is almost equipotential and the field enhancement is analogical to the one produced by a conductor. Moreover, the image method can not be applied for materials with finite conductivity. We emphasize that although the perfect conductivity is an approximation, it allows to perform important parametric studies using fast, image method based, solutions that would not be possible in framework of other model approaches. Thus, the spheres are considered to be conductors as in our previous work (Cai et al., 2017). The schematics is shown in Figure 1. The approach is described in detail in Appendix A1. The two conducting spheres with different radii R_1 and R_2 are separated with the gap of length s. The uniform applied electric field E_0 is created by positioning two source charges $\pm Q$ at remote locations $z = \mp R_Q$ (Jackson, 1999, p. 63). In the limit $R_Q \to \infty$, the charge magnitude $Q = 2\pi\varepsilon_0 E_0 R_Q^2$ produces a uniform thundercloud electric field E_0 parallel to the z axis in the region





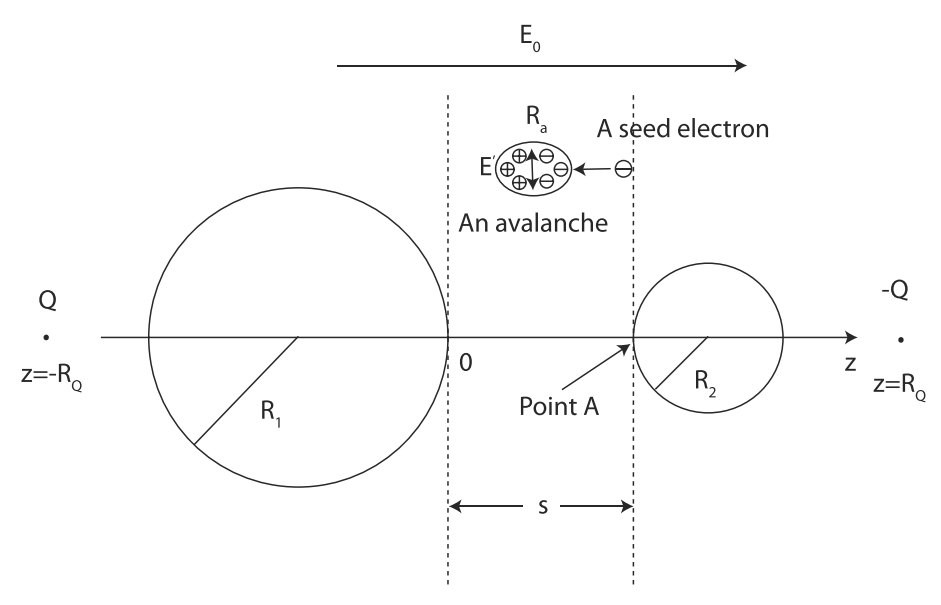


Figure 1. The schematics of two uncharged spheres with different radius in a uniform electric field.

of interest pointing in the direction from Sphere 1 toward Sphere 2. The electric field in the gap is calculated from the gradient of the potential obtained from the image charge series in these two spheres. The resultant electric field can be seen in Figure 2. If the electric field in the whole gap is larger than the breakdown electric field E_k (i.e., ~28.7 kV · cm⁻¹ · atm⁻¹, Morrow & Lowke, 1997), the avalanche would originate from the seed electron on the surface of Sphere 2 and propagate in the opposite direction of E_0 as depicted in Figure 1. In order to analyze avalanche-to-streamer transition, we use the Meek criterion (e.g., equation (11), Babich et al., 2016):

$$\int_0^s \left(\alpha_{\text{ion}}(E(z)) - \alpha_{\text{att}}(E(z)) \right) dz = M, \tag{1}$$

where M is the Meek number, $\alpha_{\rm ion}$ and $\alpha_{\rm att}$ are the ionization and the two-body dissociative attachment coefficients, respectively, taken from Morrow and Lowke (1997). To analyze similar problematics, recently Cai et al. (2017) used M=20 (Babich et al., 2016), and a more accurate numerical model developed in Qin et al. (2011) for studies of avalanche-to-streamer transition. Both methods are based on consideration of a single electron avalanche growing until it disturbs external electric field due to its own space charge effects. Naidis (2005) and Liu, Dwyer, and Rassoul (2012) studied conditions for positive corona initiation around spherical particles including the process of a photoionization feedback. The essence of the photoionization feedback is that

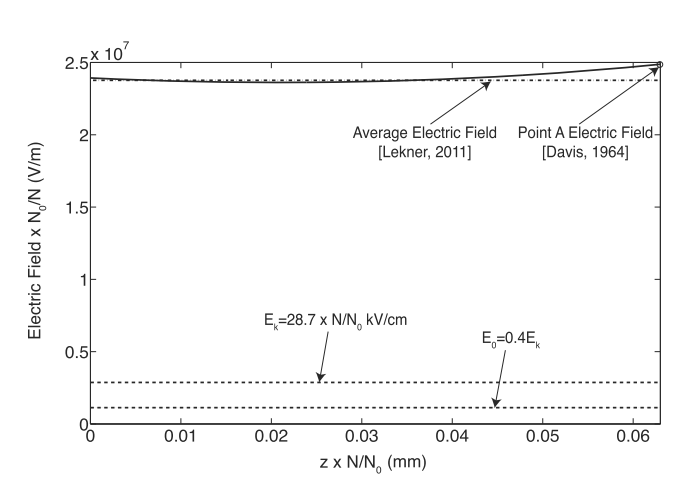


Figure 2. Electric field between two spheres for $R_2 = 0.8 N_0/N$ mm, $R_1 = 2R_2$, $s = 0.079 R_2$, and $E_0 = 0.4E_k$.

the initial avalanche produces photons, which can generate secondary electrons in the surrounding volume and cause additional avalanches. These avalanches allow for streamer initiation at a lower applied field. Liu, Dwyer, and Rassoul (2012) followed methodology developed in Naidis (2005) for positive corona inception in air around one spherical electrode. Naidis (2005) evaluated the parameter K (ionization integral characterizing the electron avalanche growth), which is equivalent to M in this paper, for the discharge inception criterion. For a parameter of K higher than the threshold for the corona onset stage, the corona discharge transitions into the streamer stage. Jánský and Pasko (2017) reported the thresholds for streamer ignition between and outside of hydrometeors. Jánský and Pasko (2017) used a streamer model to provide an accurate solution of the ignition criterion for two hydrometeor scenarios. Their streamer model is more accurate than the above mentioned method (Liu, Dwyer, & Rassoul, 2012), but it is also much more time-consuming. Therefore, the criterion is determined only for specific hydrometeor geometry. The advantage of a streamer model is also that it shows streamer ignition and not just positive corona threshold. Jánský and Pasko (2017) focused on the geometry

for streamer ignition between two hydrometeors, which is at an air neutral density of $0.5 N_0$ and an ambient electric field of $0.5 E_k$ with $R_1 = 3$ mm and $R_2 = 1$ mm. The threshold is estimated to be 12 for this particular geometry. We note that as expected, it is much smaller than the classical Meek criterion of 18-20, but higher than the Meek number of K=8 for photoionization feedback with a single hydrometeor of R=3 mm at air neutral density 0.5 N_0 (Naidis, 2005, Figure 1). As for the study of the ignition of the streamer discharge outside of the right hydrometeor with radius R_2 , in order to compare it with the threshold for a single hydrometeor 7-9 (Liu, Dwyer, & Rassoul, 2012, Figure 4), Jánský and Pasko (2017) varied the radius of the left hydrometeor R_1 while keeping a constant radius of $R_2 = 1$ mm, a separation of s = 0.4 mm at air neutral density 0.5 N_0 , and an ambient electric field of $0.5 E_k$. Thus, the threshold for the Meek number is approximated as 8 for given hydrometeor geometry. In our work, we focus on finding the relationship between R_1 and R_2 for streamer initiation when the applied electric field is larger than the minimum field required for propagation of positive streamers in air E_{cr}^+ (i.e., $E_{cr}^+ \simeq 4.4$ kV/cm $\simeq 0.15$ E_k at ground level, Allen & Ghaffar, 1995). We investigate a range of values between 0.2 E_k and 0.5 E_k , since if the electric field is higher than E_{cr}^+ , the streamer-to-leader transition would be likely to occur (Cai et al., 2017). For example, we note that when $R_1 = R_2 = 0.8 N_0/N$ mm, where N_0 is air density at ground level and N is air density at an altitude of interest, it is possible that avalanche to streamer transition occurs under an applied field of 0.4 E_k . In our simulations, R_1 and R_2 are sampled from $0.05 N_0/N \, \mathrm{mm}$ to $3 N_0/N \, \mathrm{mm}$ with steps of $0.05 N_0/N \, \mathrm{mm}$. s/R_2 is varied from 10^{-3} to 10^0 where the exponent is sampled from -3 to 0 with a step of 0.1. We then calculate the Meek number M as a function of R_1 , R_2 , and s/R_2 , and the results are effectively represented in the form of a lookup table. Since for colliding particles we can assume that all possible values of separations s/R_2 are realized, our goal is to document all R_1 and R_2 combinations leading to streamer initiation in accordance with a $M \ge M_{\rm i} = 12$ criterion. For all cases, we assume the locations of two source charges for producing the uniform applied electric field $R_0 = 1,000 \, \text{min} \, (R_1,R_2)$ and spatial resolution $\Delta z = \min (R_1, R_2)/10,000$, and we perform 30 iterations using the image method. Additional tests demonstrated that 30 iterations provide accurate solutions for electric fields for all considered cases.

2.2. Electric Field of Two Connected Uncharged Spheres in a Uniform Electric Field

The physical setup considered in this subsection represents a situation when two spheres are connected using a streamer channel. We use the image method to get the solution for the electric field at the outer periphery of Sphere 2 along z axis. The details of the image method are provided in Appendix A2. Since streamer initiation in the gap must occur before the one at the outer periphery, we use the lookup table previously mentioned in section 2.1 with a Meek number of 12 to find the largest separation s_{max} for streamer initiation between the spheres, using the same parametric space for R_1 , R_2 , and s/R_2 as defined in section 2.1. Then, based on these results, we calculate the electric field at the outer periphery of Sphere 2 that corresponds to a Meek number $M \ge M_0$, $M_0 \approx 8$ for given R_1 , R_2 , and s_{max} . The condition for streamer initiation outside Sphere 2 $M \ge M_0$, $M_0 \approx 8$ is supported by separate numerical simulations (Jánský & Pasko, 2017). The numerical outside threshold value $M_0 \approx 8$ is significantly lower than $M_1 \approx 12$ obtained for the streamer initiation between spheres and is a representation of larger volume available for the photoionization feedback outside of Sphere 2 in comparison with the relatively small gap between spheres. For all cases, R_Q , spatial resolution, Δz , and the iteration number for the image method are the same as in section 2.1. We choose representative ambient electric field values spanning from just above E_{cr}^+ and up to half of E_k : $0.2E_k$, $0.3E_k$, $0.4E_k$, and $0.5E_k$.

2.3. Frequency of Streamer Initiation

In order to estimate the possibility of the scenarios when avalanche-to-streamer transition occurs, we use a hard-sphere collision model (Lieberman & Lichtenberg, 2005, p. 45). Thus, for a collision between spheres with given R_1 and R_2 the cross section is approximated as $\sigma = \pi(R_1 + R_2)^2$ (equation (3.1.4), Lieberman & Lichtenberg, 2005). Note that the units of σ are m². The rate constant is defined as $K = \sigma v_r$ (equation (3.1.9), Lieberman & Lichtenberg, 2005), where v_r is relative velocity of particles with units of meters per second. Then, based on equation (2) Dye et al. (1986), the collision rate ΔC_R between particles of radius R_1 and R_2 in size intervals, ΔR_1 and ΔR_2 , is

$$\Delta C_{\rm R} = N(R_1)N(R_2)K\Delta R_1\Delta R_2,\tag{2}$$

where $N(R_1)$ and $N(R_2)$ are concentrations of particles with radius R_1 and R_2 , respectively. Note that the quantity N(R) is the concentration of particles with a radius between R and $R + \Delta R$, where the units of N(R)

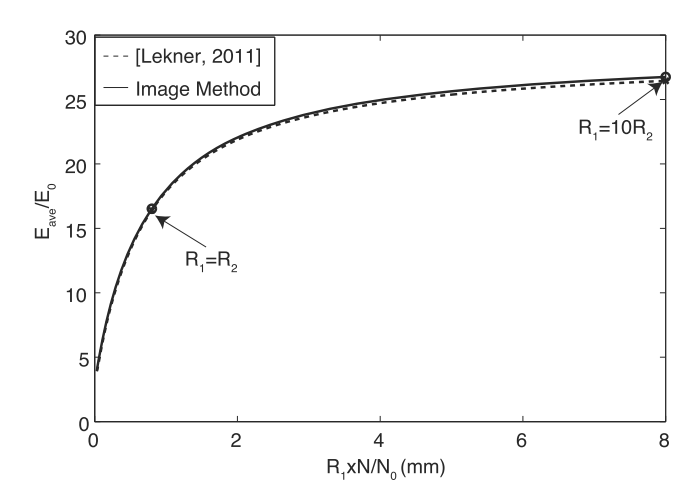


Figure 3. The ratio of average field to applied field E_{ave}/E_0 as a function of R_1 for $R_2 = 0.8 \, N_0/N$ mm and $s = 0.079 \, R_2$.

are m^{-3} mm⁻¹ and the units of R are mm. Thus, the total collision rate C_T for all particles combinations for streamer initiation can be written as (in units m^{-3}/s)

$$C_{T} = \int\!\!\int_{S(R_{1},R_{2})} N(R_{1})N(R_{2})KdR_{1}dR_{2}, \tag{3}$$

where S represents the area on (R_1, R_2) plane where the combinations of R_1 and R_2 satisfy streamer initiation, as discussed in further sections of this paper.

Since we are interested in the number of collisions corresponding to avalanche-to-streamer transition for a given region, we need to consider its volume V. Therefore, the total collision frequency v_t can be obtained as (in units 1/s)

$$v_{t} = C_{T}V, \tag{4}$$

where the unit of volume V is m^3 . For numerical estimates, we adopt relative velocity of particles $v_r = 20$ m/s based on the measurements of mean horizontal velocity of precipitation particles (Fukao et al., 1985). If we use

the equation (20) from Wisner et al. (1972) with the diameter D=3 mm, the density of ice $\rho_{ice}=900$ kg/m³, the drag coefficient $C_D = 0.4$ and the density of air $\rho_{\rm air} = 1.4$ kg/m³, the terminal velocity is $\simeq 8$ m/s, which would not influence the order of our results significantly. The inference of relative velocity of particles from the microwave radar measurements (Fukao et al., 1985) or the terminal velocity estimates (Wisner et al., 1972) is a simplifying assumption of the present modeling. We emphasize, however, that other parameters like volume of thundercloud with enhanced electric field and size distributions of hydrometeors (inherently exponential) play a more important role in quantitative results reported in the present work. Additionally, we choose a volume $V = 10^3$ m³ that represents a very localized region with dimension $10 \text{ m} \times 10 \text{ m} \times 10 \text{ m}$ adequate for leader formation as determined by Cooray (2015). We use three representative particle distributions. First, the N(R) can be represented as $N(R) = N_0 e^{-\Lambda 2R}$, where $\Lambda = 4.1 r^{-0.21}$ and r is the rate of rainfall with the unit, of mm/hr (Marshall & Palmer, 1948). We consider raindrop distribution in a strong thunderstorm with $r=25~{\rm mm^{-1}~hr^{-1}}$, which gives $N_0=8,000~{\rm m^{-3}~mm^{-1}}$ and $\Lambda=2.09~{\rm mm^{-1}}$ (Marshall & Palmer, 1948). We also use two measured distributions for thunderstorms from (Waldvogel, 1974) with $N_0 = 35,000 \text{ m}^{-3} \text{ mm}^{-1}$ and $\Lambda = 3.7 \text{ mm}^{-1}$, and 4,000 m⁻³ mm⁻¹ and $\Lambda = 2.5 \text{ mm}^{-1}$, respectively. Figure 9 illustrates particle concentrations as a function of diameter D in a classical format. Note that the hydrometeor distributions used in the present paper are different from the one based on Auer (1972), which is used in Cai et al. (2017). The connection between our results and those from Cai et al. (2017) is discussed in section 3.3. In addition, turbulent fluctuations and intermittency in hydrometeor distributions can significantly increase the ambient electric field in thunderclouds and further increase the possibility of streamer initiation (ludin, 2017).

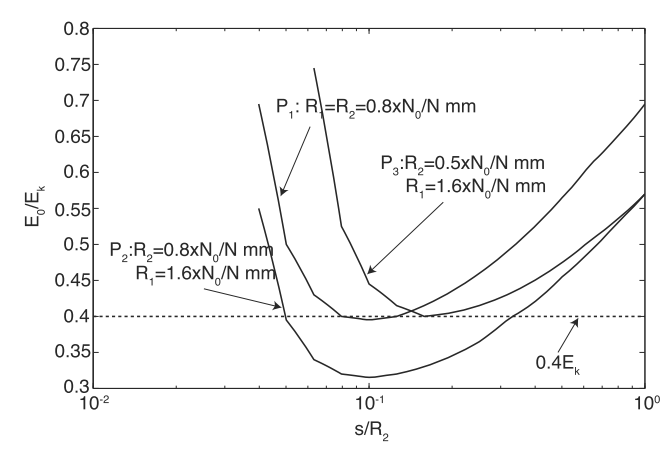


Figure 4. The electric field for avalanche-to-streamer transition between two spheres as a function of s/R_2 for different radius combinations.

3. Results and Discussion

3.1. Two Separated Uncharged Spheres in a Uniform Field

The electric field in the gap on the axis of symmetry between two spheres is illustrated in Figure 2 assuming $R_2=0.8\,N_0/N$ mm, $R_1=2R_2$, $s=0.079\,R_2$, and $E_0=0.4E_k$. Compared with a field for two spheres with the same radii (Cai et al., 2017, Figure 2a), the field is asymmetric with respect to the middle of the gap. The maximum electric field is at the surface of the smaller sphere (i.e., R_2 in Figure 1) and exhibits a minimum value on the left side with respect to the center of the gap. The field in the gap is substantially higher than the breakdown field E_k . Davis (1964) and Lekner (2011) provided the maximum electric field $E_{\rm max}$ and average electric field $E_{\rm ave}$ in the gap by solving the Laplace's equation in bispherical coordinates. The formulae are summarized in Appendix B, and the comparison with our results is shown in Figure 2. In our work, the average electric field is enhanced by a factor of ~20.8 with respect to E_0 and this number agrees well with the field enhancement factor

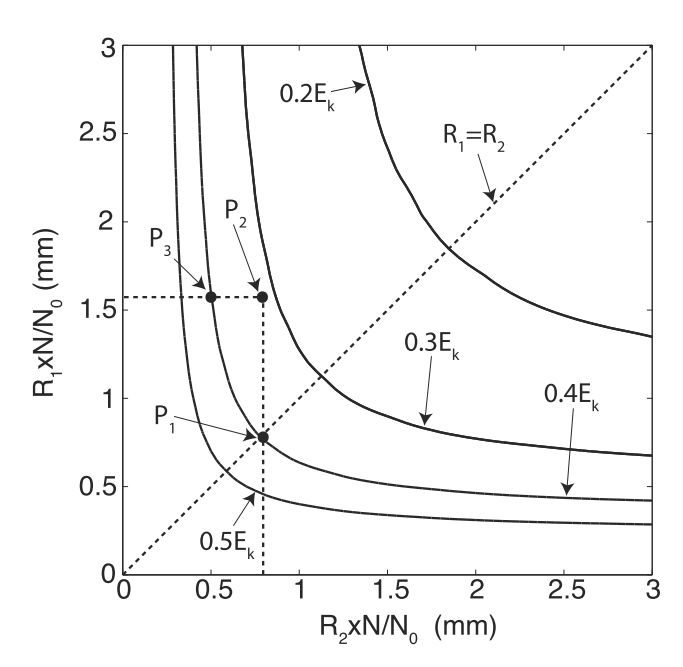


Figure 5. R_1 as a function of R_2 for avalanche-to-streamer transition under applied electric fields $0.2E_k$, $0.3E_k$, $0.4E_k$, and $0.5E_k$.

(Lekner, 2011, equation (B10), which is \sim 20.7. We also note that the maximum electric field at Point A is enhanced by a factor of \sim 21.7 with respect to E_0 , which is approximately the same as the one calculated based on Davis (1964; \sim 21.6).

In order to illustrate the influence of variation of the radius on the electric field in the gap, we look at the relationship between the radii of these two spheres and amplification factors E_{ave}/E_0 . Moreover, in order to check the accuracy of our solutions, we make a comparison between our results and the analytical solutions from Lekner (2011) by keeping R_2 constant as $0.8 N_0/N$ mm, $s = 0.079R_2$ and varying R_1 from $0.05R_2$ to $10R_2$. As shown in Figure 3, our results based on the image method agree very well with the results from Lekner (2011). When $R_1 = R_2$, the electric field amplification factor E_{ave}/E_0 (indicated by circle) is ~16.4, which is close to ~16.3 (indicated by cross) based on Lekner (2011). When $R_1 = 10R_2$, our result (\sim 26.8) is also close to the result from Lekner (2011; \sim 26.4). We find that with the increase of R_1 , the amplification factor increases. Considering the symmetry of the two sphere system, if we keep R_1 and the length of the gap the same and increase R_2 , the electric field amplification factor would similarly increase. In other words, increasing the radius of either one of these two spheres would increase the amplification factor.

In order to further explore the influence of variation of radius on the avalanche-to-streamer transition, Figure 4 shows the applied electric field

necessary for streamer initiation as a function of s/R_2 for different radii of hydrometeors using $M_i=12$ as a threshold. From Figure 4, we find that when $R_1=R_2=0.8\,N_0/N$ mm, the minimum applied electric field for avalanche-to-streamer transition is equal to $0.4E_k$. If we increase R_1 by a factor of 2, based on the results shown in Figure 3, we know that the amplification factor would increase such that the applied electric field required for streamer initiation would decrease, which shifts the curve downward. Then, if we keep $R_1=1.6\,N_0/N$ mm (i.e., twice of previous R_2 value), we need to decrease R_2 from 0.8 to $0.5\,N_0/N$ mm so that the minimum electric field is increased and again close to $0.4E_k$.

Thus, in order to investigate the influence of the magnitude of the applied electric field on the variations related to R_1 and R_2 , we use a different applied electric field (i.e., $0.2E_k$, $0.3E_k$, $0.4E_k$, and $0.5E_k$) to find the combinations of R_1 and R_2 corresponding to streamer initiation. From Figure 5, we find that these four curves are symmetric with respect to $R_1 = R_2$ due to the symmetry of our model. We also find that for the higher electric field applied, the lower radii allowed for streamer initiation. If the radii of hydrometeors are the same, the lower the radii, the lower electric field amplification factor in the gap such that a higher applied electric

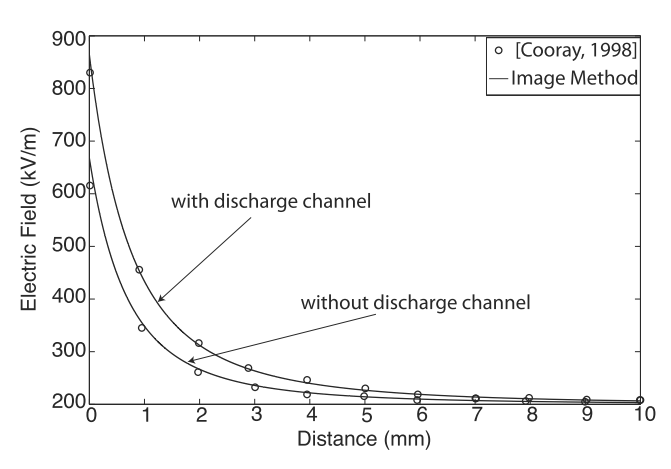


Figure 6. Electric field as a function of distance from the outer end of the water drop for a system of two drops. Background field 200 kV/m, drop radius 2 mm, and gap 0.39 mm.

field is required. Note that P_1 , P_2 , and P_3 indicate the three combinations of two different radii of hydrometeors shown in Figure 4. From Figure 3, we know that increasing the radius of either one of these two spheres would increase the amplification factor. Therefore, all R_1 and R_2 combinations in regions above the curves in Figure 5 indicate that avalanche-to-streamer transition would occur under the applied electric field corresponding to each of the curves.

3.2. Two Connected Uncharged Spheres in a Uniform Field

The streamer propagating between spheres impacts the Sphere 2 and causes electrical connection of two particles. Cooray et al. (1998) indicate that the connection of two particles by a discharge channel would increase the electric field at the outer periphery of the two particles above the field caused by a single particle or two particles without the connecting discharge. Therefore, in this section we analyze the scenario when the two particles are connected by a discharge channel and study when the streamer can ignite on the outer periphery. Such a streamer may have enough space to propagate under the applied electric field above E_{cr}^+ , which allows for growth of streamer and formation of streamer corona.



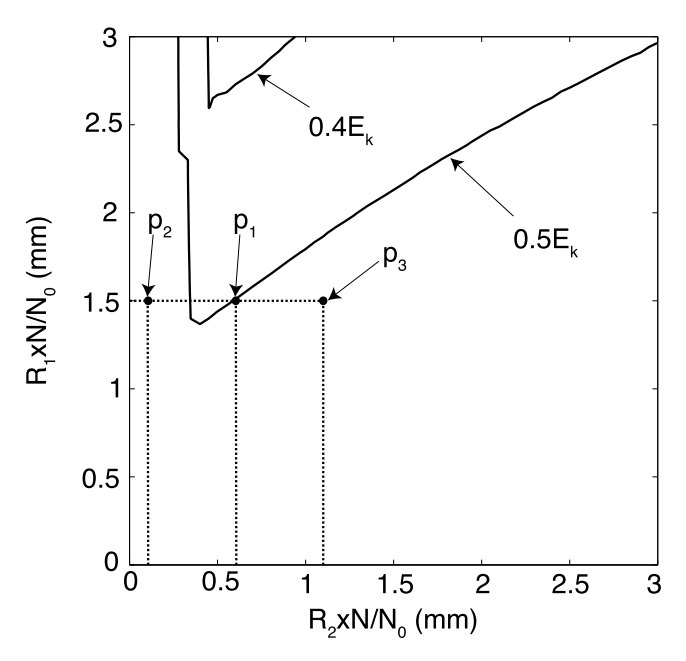


Figure 7. R_1 as a function of R_2 for streamer initiation outside of sphere 2 under applied electric field $E_0 = 0.4E_k$ and $0.5E_k$.

Experiments at ground pressure have shown that leaders are initiated when the length of streamer corona is \sim 1 m (Raizer, 1991, p. 366). In order to verify our results based on the image method described in section 2.2 and Appendix A2, we compare our results with Cooray et al. (1998, Figure 4). These are shown by circles in Figure 6. We find that our results agree well with the ones from Cooray et al. (1998) for two particles with and without a discharge channel.

In order to investigate streamer initiation outside of these two spheres, we search for the relationship between R_1 and R_2 under applied electric fields of $0.2E_k$, $0.3E_k$, $0.4E_k$, and $0.5E_k$. We calculate the electric field at the outer periphery of Sphere 2 and obtain the relationship between R_1 and R_2 following the methods described in section 2.2. In particular, to characterize streamer initiation, we use a threshold value for a Meek number $M_o \simeq 8$. The results are shown in Figure 7 and indicate that R_1 as a function of R_2 initially decreases and then increases after achieving a minimum value. Furthermore, we emphasize that for R_1 and R_2 in the range of 0.0/N to 3.0/N mm, only $0.4E_k$ and $0.5E_k$ allow for streamer initiation. All R_1 and R_2 combinations in regions above these two curves satisfy the streamer initiation criterion. We note that these regions represent only a small fraction of R_1 and R_2 parametric space corresponding to streamer initiation between spheres as shown in Figure 5.

In order to further understand the minimum value of R_1 as a function

of R_2 , in Figure 8, we keep constant $R_1 = 1.5 \, N_0/N$ mm and separation $s = 0.0474 \, N_0/N$ mm and then modify R_2 . Note that p_1 , p_2 , and p_3 correspond to those points indicated in Figure 7. When $R_2 = 0.6 \, N_0/N$ mm, the Meek number is $M = M_0 = 8$, and the streamer is initiated. When we decrease R_2 to $0.1 \, N_0/N$ mm, the streamer is not initiated. Under these conditions M = 6.8. Even though the electric field at the surface of Sphere 2 increases, the electric field decreases sharply with distance from Sphere 2 such that the length of the avalanche propagation is short, leading to a decrease of M. Also if we increase R_2 to $1.1 \, N_0/N$ mm, the streamer is not initiated. The length of avalanche propagation increases, while the surface electric field decreases, which results in $M = 5.5 \, (< M_0)$.

3.3. Streamer Initiation Frequency

Previous sections 3.1 and 3.2 provide us with solutions when streamer ignition is possible for two particles with given radii R_1 and R_2 . To evaluate whether this scenario can be responsible for lightning initiation, the measured particle size distributions inside thunderstorms are combined with our simulated particle radii. In order to investigate the possibility of scenarios shown in Figures 5 and 7, we calculate the frequency for streamer initiation v_t using equation (4), and three particle size distributions shown in Figure 9. Note that if we calculate the collision frequency using the distribution based on Auer (1972) for the same radius $R_1 = R_2 = 3$ mm,

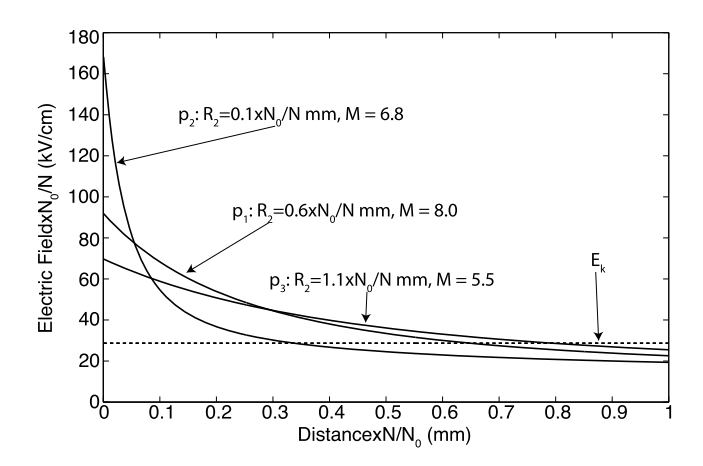


Figure 8. Electric field as a function of distance for constant $R_1 = 1.5 N_0/N$ mm and $s = 0.0474 N_0/N$ mm and different $R_2 = 0.1$, 0.6 and $1.1 N_0/N$ mm.



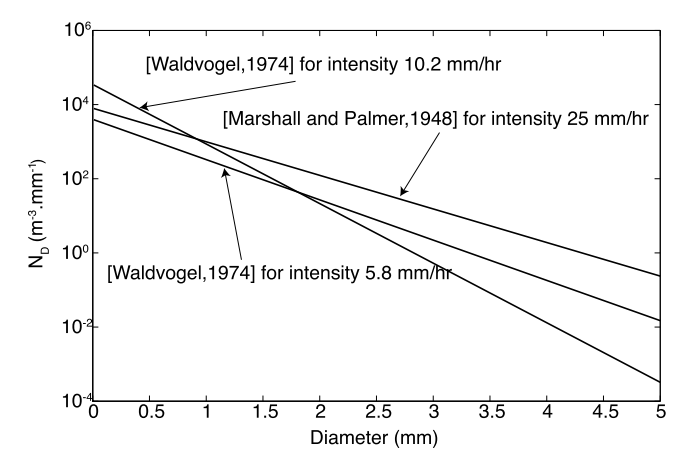


Figure 9. Rain spectra as a function of diameter D of raindrop.

we would get collision frequencies $\sim 5.8 \times 10^5$ 1/s for the region with dimension of 2 km \times 0.1 km \times 0.8 km, and ~3.6 1/s for the region with dimension of 10 m, respectively, which are the same as the results reported in Cai et al. (2017). According to Stolzenburg et al. (2007), the duration of electric field increase in lightning flashes is 1-5 s. Therefore, we use the minimum frequency 1 Hz (i.e., requiring one or more collision events per second) as the threshold to determine whether these scenarios are realistic. Results presented in Table 1 indicate that a streamer can be initiated in the gap between two colliding hydrometeors at 0-km altitude when the applied electric field E_0 is larger than $0.3E_k$ for the rain spectra of Waldvogel (1974) and when the applied electric field E₀ is larger than 0.2E, for the rain spectra of Marshall and Palmer (1948; i.e., for these parameters the frequency is larger than 1 Hz). Table 2 shows that for the streamer initiation outside of Sphere 2, when the applied electric field is 0.4E_k at 0 km and the rain spectra are based on Marshall and Palmer (1948), the frequency can achieve 4.6 Hz. The other models do not lead to streamer initiation. Table 2 indicates that for applied electric fields $0.5 E_k$ at 0-km altitude all three models lead to streamer initiation. In order to investigate streamer initiation outside of Sphere 2 at real-thundercloud altitudes, we consider representative altitudes of 3 and 6 km since according to Rakov and Uman (2003, p. 79, Table 3.9), the lightning discharge initiated from the lower positive charge center and the main negative charge center mainly occurs at these altitudes in thunderclouds. Results presented in Table 2 indicate that at an applied electric field $0.4 E_k$ none of the three models can lead to streamer initiation at altitudes of 3 and 6 km. For an applied field $0.5 E_{k}$, Table 2 indicates that at 3 km, two out of three distributions give a value higher than 1 Hz, and at 6 km, only distribution based on Marshall and Palmer (1948) gives a value higher than 1 Hz. Based on the results shown in Table 2, we conclude that the scenarios for lightning initiation are realistic only at a high field $\sim 0.5E_{\nu}$. We emphasize that this field exceeds measured fields in thunderclouds.

Table 1Frequency of Streamer Initiation (in Hz) Under Different Applied Fields 0.2E_k, 0.3E_k, 0.4E_k, and 0.5E_k Calculated Using Different Rain Spectra Models at 0 km

Source	Waldvogel (1974)(10.2)	Waldvogel (1974) (5.8)	Marshall and Palmer (1948) (25)
$N_0e^{-\Lambda D}$	$35000e^{-3.7D}$	$4000e^{-2.5D}$	$8000e^{-2.09D}$
0.2 <i>E</i> _k	1.3×10^{-4}	2.3×10^{-2}	2.6
0.3 <i>E</i> _k	1.9	11	4.1×10^{2}
0.4 <i>E</i> _k	1.4×10^{2}	1.6×10^{2}	3.4×10^{3}
0.5 <i>E</i> _k	1.4×10^{3}	6.7×10^{2}	1.0×10^4

Note. The $\Lambda=4.1r^{-0.21}$ and r is the rate of rainfall with the units of mm/hr, which are the values in brackets in Table 1. Additionally, the units of N_0 are m⁻³ mm⁻¹.

Table 2Frequency of Streamer Initiation (in Hz) Outside of Sphere 2 After Spheres Connected With Discharge Channel Under Different Applied Field $0.4E_k$ and $0.5E_k$ Calculated Using Rain Spectra Models at 0, 3 and 6 km

Model	0.4 <i>E</i> _k	0.5 <i>E</i> _k
0 km	1.2×10^{-3} a	12 ^a
	6.1×10^{-2b}	24 ^b
	4.6 ^c	602 ^c
3 km	2.6×10^{-7a}	1.4×10^{-1} a
	2.4×10^{-4} b	1.3 ^b
	5.0×10^{-2} c	59 ^c
6 km	1.2×10^{-12a}	1.8×10^{-4a}
	7.1×10^{-8b}	1.9×10^{-2b}
	6.4×10^{-5} c	1.8 ^c

^aWaldvogel (1974) (10.2). ^bWaldvogel (1974) (5.8). ^cMarshall and Palmer (1948) (25).

As shown in Figure 9, particle distributions decrease exponentially with increasing radii. Considering this dependence within equation (1) for the frequency of streamer initiation, it is observed that particles with radii (around minimum of curve $R_1 = f(R_2)$ in Figure 7), $R_1 \sim 1.5 N_0/N$ mm and $R_2 \sim 0.5 \, N_0 / N \, \text{mm}$, will contribute most to the streamer initiation. Liu, Kosar, et al. (2012) used $0.5E_{k}$ for streamer initiation from an isolated ionization column. Sadighi et al. (2015) made an improvement and indicated that it is possible that a stable streamer is initiated from thundercloud hydrometeors in a $0.3 E_{\nu}$ electric field. Therefore, the applied electric field $0.5 E_{\nu}$ obtained from our results is consistent with the minimum in the range of electric field values required for streamer initiation that are discussed in previous publications. Note that we calculate the results in Tables 1 and 2 using a very localized volume. The streamer initiation frequency is proportional to volume. If we estimate the frequencies using $2 \text{ km} \times 0.1 \text{ km} \times 0.8 \text{ km}$ based on Proctor (1991), the results would be multiplied by 160,000 such that when the applied field is $0.4E_k$, an avalanche-to-streamer transition is possible (e.g., at 6 km, the frequency could be 10.2 Hz for the rain spectra based on Marshall & Palmer, 1948).

4. Conclusions

The principal results in this paper can be summarized as follows:

- We have developed the model formulation of two separated uncharged spheres with different radii in a uniform electric field and obtained the electric field in the gap between two spheres using the image method.
- 2. We have found the relationship between R_1 and R_2 for successful streamer initiation between two spherical particles.
- 3. If streamer is initiated in the gap, the streamer would propagate from Sphere 1 toward Sphere 2 such that the electrical connection between these two spheres would occur in the gap. We investigate the model of two uncharged spheres with a discharge channel in a uniform electric field. We have reproduced results of Cooray et al. (1998) for streamer initiation at the outer periphery of two spheres with same radii and connected with a discharge channel in a uniform electric field and obtained quantitative agreement with the results presented in Cooray et al. (1998).
- 4. We have found that for R_1 and R_2 in the range of $0 N_0/N$ to $3 N_0/N$ mm, the applied electric field larger than $0.4E_k$ allows for streamer initiation outside of two spheres. The corresponding radii are $R_1 \sim 3 N_0/N$ mm and $R_2 \sim 0.5 N_0/N$ mm.
- 5. We have estimated the frequency of streamer initiation based on particle dimensions for a separated two-sphere system and a connected two-sphere system and concluded that for three considered hydrometeor model distributions the streamer initiation is only possible for a relatively high electric field $\sim 0.5 E_k$ at altitudes 3 and 6 km. The most likely scenario is for two particles with radii $R_1 \sim 1.5 \, N_0/N$ mm and $R_2 \sim 0.5 \, N_0/N$ mm.

Appendix A: Electric Field Calculation Based on the Image Method

A1. Electric Field for Two Particles Without a Discharge Channel

The schematics for two separated particles is shown in Figure A1. Note that we use the terms $Q_{\rm m}(i,j)$ and $z_{\rm m}(i,j)$ to represent charges and relative locations in Sphere 1 or 2, where m (e.g., 1 or 2) represents whether the charge belongs to Sphere 1 or 2. The index j represents the iteration number, and i represents the index of charge in each sphere in the jth iteration. To better illustrate the procedures of the image method, we discuss an image charge of Q at $z=-R_Q$ in Sphere 1 as an example. In the first iteration, we have an image charge of $Q_1(1,1)=-\frac{R_1Q}{R_Q}$ with location $z_1(1,1)=-R_1-\frac{R_1^2}{R_Q}$ in Sphere 1 to keep it equipotential under the influence of charge Q. In order to keep the neutrality of Sphere 1, we place neutralization charge $Q_1(2,1)=-Q_1(1,1)$ at the center of Sphere 1 where $z_1(2,1)=-R_1$. Thus, in the second iteration, in order to keep Sphere 2 equipotential, we place two image charges $Q_2(i,2)=-\frac{R_2Q_1(i,1)}{s+R_2-z_1(i,1)}$ with locations $z_2(i,2)=s+R_2-\frac{R_2^2}{s+R_2-z_1(i,1)}$ (i=1,2). To preserve its neutrality, we place $Q_2(3,2)=-\sum_{i=1}^{2}Q_2(i,2)$ in the center of Sphere 2 where $z_2(3,2)=s+R_2$.





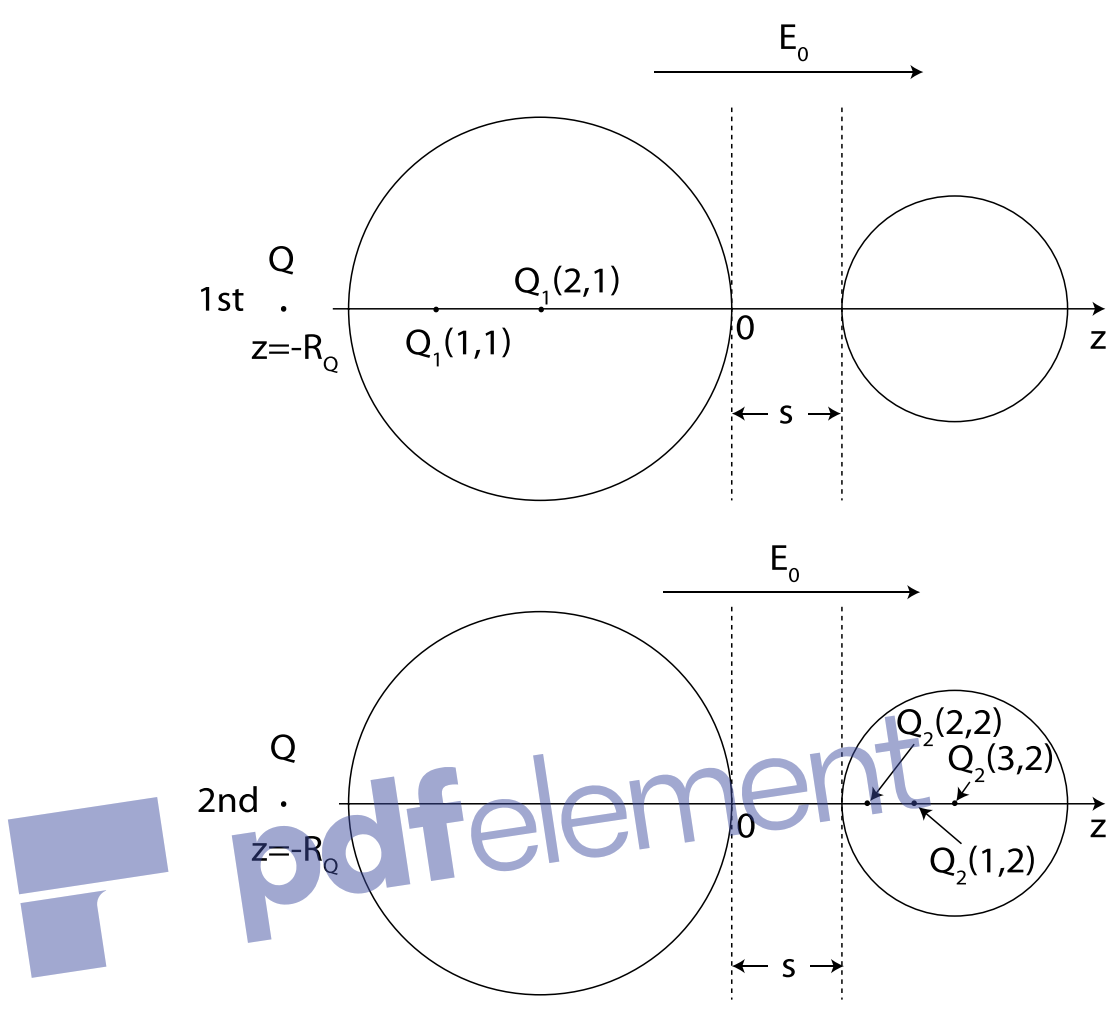


Figure A1. The schematics for evaluating electric field in the gap of two particles without a discharge channel using the image method.

It is easy to find that in the (2k-1)th iteration, 2k charges would be introduced to Sphere 1, and in the (2k)th iteration, 2k+1 charges would be introduced to Sphere 2, where $k=1,2,3,4,\ldots$ For (2k-1)th $(k=2,3,4,\ldots)$ iteration, the image charges in Sphere 1 can be represented as

$$Q_{1}(i_{1}, 2k - 1) = -\frac{R_{1}Q_{2}(i_{1}, 2k - 2)}{z_{2}(i_{1}, 2k - 2) + R_{1}}, i_{1} = 1, 2, \dots, 2k - 1$$

$$z_{1}(i_{1}, 2k - 1) = -R_{1} + \frac{R_{1}^{2}}{z_{2}(i_{1}, 2k - 2) + R_{1}}, i_{1} = 1, 2, \dots, 2k - 1$$
(A1)

and the relative neutralization charges in Sphere 1 can be represented as

$$Q_1(i_1, 2k - 1) = -\sum_{i=1}^{2k-1} Q_1(i, 2k - 1), i_1 = 2k$$

$$Z_1(i_1, 2k - 1) = -R_1, i_1 = 2k$$
(A2)

Similarly, for (2k)th (k = 2, 3, 4, ...) iteration, the image charges in Sphere 2 can be represented as

$$Q_{2}(i_{2}, 2k) = \frac{-R_{2}Q_{1}(i_{2}, 2k - 1)}{-z_{1}(i_{2}, 2k - 1) + s + R_{2}}, i_{2} = 1, 2, \dots, 2k$$

$$z_{2}(i_{2}, 2k) = s + R_{2} - \frac{R_{2}^{2}}{-z_{1}(i_{2}, j) + s + R_{2}}, i_{2} = 1, 2, \dots, 2k$$
(A3)



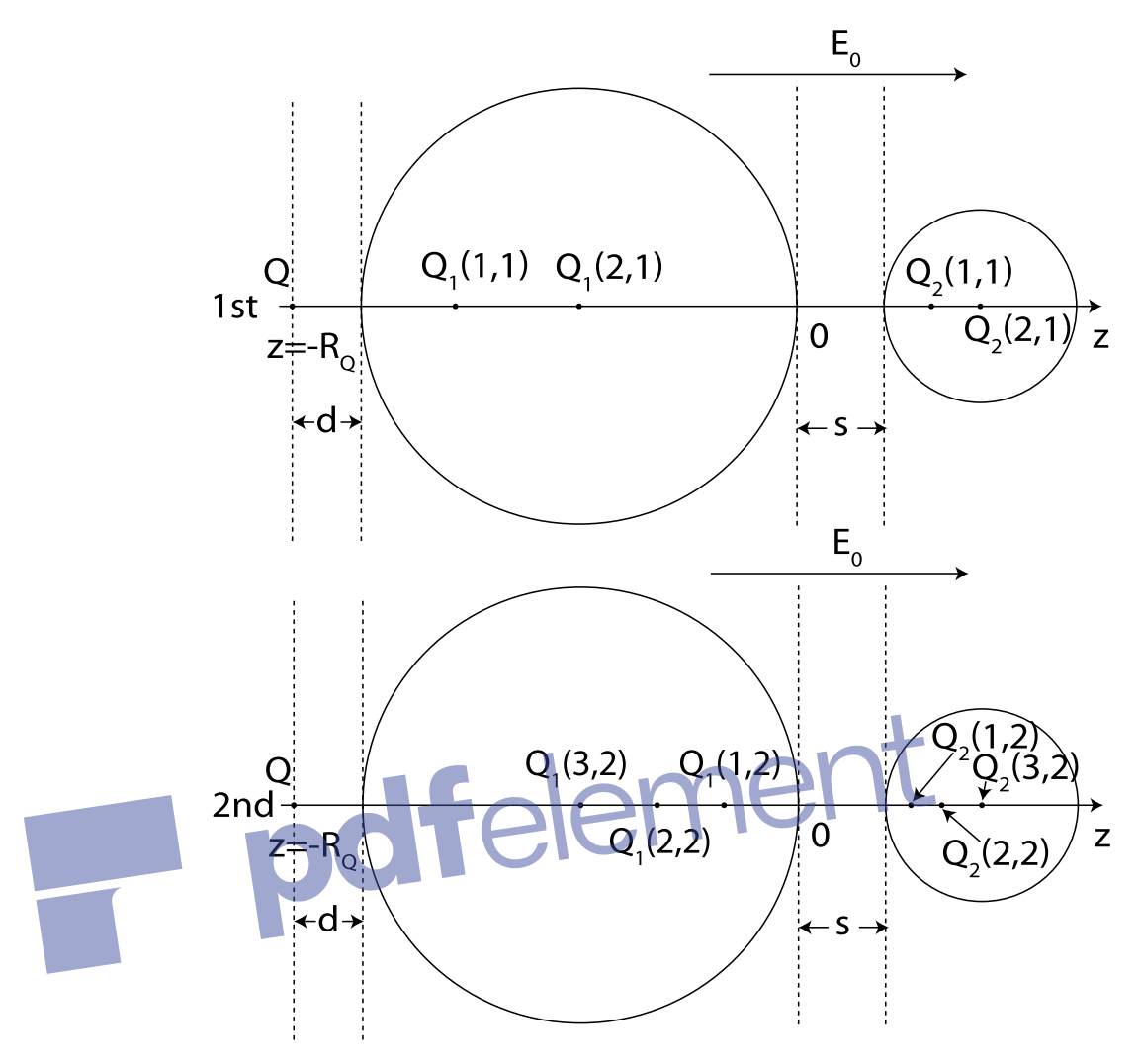


Figure A2. The schematics for evaluating outside electric field of two particles with a discharge channel using the image method.

and the relative neutralization charges in Sphere 2 can be represented as

$$Q_2(i_2, 2k) = -\sum_{i=1}^{2k} Q_2(i, 2k), i_2 = 2k + 1$$

$$z_2(i_2, 2k) = s + R_2, i_2 = 2k + 1$$
(A4)

Using the equations mentioned above, we can also find the charge series for Sphere 1 and Sphere 2 that resulted from images of -Q at $z=R_Q$ in Sphere 1 and Sphere 2, and images of Q at $z=-R_Q$ in Sphere 2. We can find the potential in the gap between the two spheres by summing up the potential produced by all the image and neutralization charges in every iteration and then find the electric field in the gap by calculating the negative gradient of the potential. Note that the iteration number should be large enough to guarantee the convergence of the solution.

A2. Electric Field for Two Particles With a Discharge Channel

The schematics for two particles with a discharge channel in a uniform electric field is shown in Figure A2. We use the terms $Q_{\rm m}(i,j)$ and $z_{\rm m}(i,j)$ to represent charges and relative locations in Sphere 1 or 2 with the same notation as in Appendix A1. Note that the precision of defining the location of the initial charges would influence the accuracy of the electric field at the outer periphery of these two particles significantly. We introduce d to represent the distance between the remote charge Q and the outer surface of Sphere 1 or 2 such that the charge magnitude $Q = 2\pi\varepsilon_0 E_0 (d + R_1 + R_2 + \frac{5}{2})^2$. In order to illustrate this method, we take



image charges resulting from the left side charge Q as an example. In the first iteration, we have an image charge of $Q_1(1,1)=-\frac{R_1Q}{d+R_1}$ with location $z_1(1,1)=-R_1-\frac{R_1^2}{d+R_1}$ in Sphere 1 and $Q_2(1,1)=\frac{-R_2Q}{d+2R_1+s+R_2}$ with location $z_2(1,1)=s+R_2-\frac{R_2^2}{d+2R_1+s+R_2}$ to keep each particle equipotential under the influence of charge Q. Now both spheres are at a potential of U=0, but the total charge of the system is generally not zero. We introduce $Q_1(2,1)$ and $Q_2(2,1)$ in the center of each particle to satisfy the relationship $\frac{Q_1(2,1)}{R_1}=\frac{Q_2(2,1)}{R_2}$ guaranteeing the same potential of both spheres. Combined with the condition that the total charge is zero, we can find that $Q_1(2,1)=-\frac{R_1}{R_1+R_2}(Q_1(1,1)+Q_2(1,1))$ and $Q_2(2,1)=-\frac{R_2}{R_1+R_2}(Q_1(1,1)+Q_2(1,1))$. In the second iteration, these two charges in Spheres 1 and 2 produce another two image charges in Spheres 2 and 1, respectively. We introduce the third charge $Q_1(3,2)$ and $Q_2(3,2)$ to keep the two particle system equipotential and the total charge zero. We can find that in the jth iteration, j+1 charges would be introduced to Sphere 1 and Sphere 2, respectively. For the jth $(j=2,3,4,\ldots)$ iteration, the image charges in Sphere 1 can be represented as

$$Q_{1}(i_{1},j) = -\frac{R_{1}Q_{2}(i_{1},j-1)}{z_{2}(i_{1},j-1) + R_{1}}, i_{1} = 1, 2, \dots, j$$

$$Z_{1}(i_{1},j) = -R_{1} + \frac{R_{1}^{2}}{z_{2}(i_{1},j-1) + R_{1}}, i_{1} = 1, 2, \dots, j$$
(A5)

and the image charges in Sphere 2 can be represented as

$$Q_{2}(i_{2},j) = \frac{-R_{2}Q_{1}(i_{2},j-1)}{-z_{1}(i_{2},j-1) + s + R_{2}}, i_{2} = 1, 2, \dots, j$$

$$z_{2}(i_{2},j) = s + R_{2} - \frac{R_{2}^{2}}{-z_{1}(i_{2},j-1) + s + R_{2}}, i_{2} = 1, 2, \dots, j$$
(A6)

Using the conditions $\frac{Q_1(j+1,j)}{R_1} = \frac{Q_2(j+1,j)}{R_2}$ and $\sum_{i=1}^{j+1} Q_1(i,j) + \sum_{i=1}^{j+1} Q_2(i,j) = 0$, we find that

$$Q_{1}(i_{1},j) = -\frac{R_{1}}{R_{1} + R_{2}} \left(\sum_{i=1}^{j} Q_{1}(i,j) + \sum_{i=1}^{j} Q_{2}(i,j) \right), i_{1} = j + 1$$

$$z_{1}(i_{1},j) = -R_{1}, i_{1} = j + 1$$
(A7)

and

$$Q_{2}(i_{1}, j) = -\frac{R_{2}}{R_{1} + R_{2}} \left(\sum_{i=1}^{j} Q_{1}(i, j) + \sum_{i=1}^{j} Q_{2}(i, j) \right), i_{2} = j + 1$$

$$z_{2}(i_{1}, j) = s + R_{2}, i_{2} = j + 1$$
(A8)

Having applied the equations mentioned above, an image charge series for Sphere 1 and Sphere 2 that resulted from charge -Q at $z=R_Q$ can be found. The potential at the outer periphery of the two spheres can be calculated by summing up the potential produced by all image and neutralization charges in every iteration, and the electric field can be obtained by calculating the negative gradient of the potential.

Appendix B: Electric Field Calculation Based on an Infinite Series Solution of Laplace's Equation

In this appendix, we summarize the results of Lekner (2011) and Davis (1964) to calculate the average electric field E_{ave} and the maximum electric field E_{max} in the gap between two spherical conductors in an external field E_0 aligned with the line connecting centers of the spheres. The model is shown in Figure 1. Davis (1964) and Lekner (2011) used bispherical coordinates (μ , η) (Morse:1953, p. 1283). Based on relations given

by Morse and Feshbach (1953, p. 1298) and Davis (1964), the two conducting spheres of radius R_1 and R_2 separated with the gap of length s illustrated in Figure 1 are characterized by $\mu = -\mu_1$ and $\mu = \mu_2$, with

$$\mu_1 = \ln\left(\frac{d_1 + a}{R_1}\right),\tag{B1}$$

$$\mu_2 = \ln\left(\frac{d_2 + a}{R_2}\right),\tag{B2}$$

where the bispherical scale factor is

$$a = \left(d_1^2 - R_1^2\right)^{\frac{1}{2}} = \left(d_2^2 - R_2^2\right)^{\frac{1}{2}},\tag{B3}$$

where d_1 and d_2 represent the distances of the centers of these two spheres from the origin of the bispherical coordinates and can be given by the following equations:

$$d_1 = \frac{1}{2h} \left(h^2 + R_1^2 - R_2^2 \right), \tag{B4}$$

$$d_2 = \frac{1}{2h} \left(h^2 + R_2^2 - R_1^2 \right), \tag{B5}$$

where $h = R_1 + R_2 + s$.

According to Davis (1964) and Lekner (2011), we obtain the potential of Sphere 1 and Sphere 2:

$$V_1 = aE_0 \frac{R_2 S_1 - R_1 S_0}{S_1 S_2 - S_0^2},$$
(B6)

 $V_{1} = aE_{0} \frac{R_{2}S_{1} - R_{1}S_{0}}{S_{1}S_{2} - S_{0}^{2}},$ $V_{2} = -aE_{0} \frac{R_{1}S_{2} - R_{2}S_{0}}{S_{1}S_{2} - S_{0}^{2}}.$ (B7)

where $U = \mu_1 + \mu_2$, $R_1 = R(U, \mu_1)$, $S_1 = S(U, \mu_1)$, $S_0 = S(U, 0)$ (and likewise for $R_2 = R(U, \mu_2)$, $S_2 = S(U, \mu_2)$) and $R(U, \mu)$ and $S(U, \mu)$ are defined as

$$R(U,\mu) = \sum_{n=0}^{\infty} \frac{(2n+1)[e^{(2n+1)\mu} + 1]}{e^{(2n+1)U} - 1},$$
(B8)

$$S(U,\mu) = \sum_{n=0}^{\infty} \frac{e^{(2n+1)\mu}}{e^{(2n+1)U} - 1},$$
(B9)

The ratio of E_{ave} , the average electric field in the gap between the two spheres, to the applied electric field E_0 (Lekner, 2011, equation (32)) is

$$\frac{E_{\text{ave}}}{E_0} = \frac{V_1 - V_2}{E_0 s} = \frac{a}{s} \frac{R_1 S_2 + R_2 S_1 - (R_1 + R_2) S_0}{S_1 S_2 - S_0^2},$$
(B10)

The electric field at point A (Davis, 1964) of Figure 1 is computed from the normal derivative

$$E_{A} = -\left(\frac{\partial V}{\partial n}\right)_{\mu = -\mu_{1}, \eta = \pi} \tag{B11}$$

Based on Lekner (2011, equation (13)), the potential function $V(\mu, \eta)$ can be written as

$$V(\mu, \eta) = \sqrt{2}(\cosh \mu - \cos \eta)^{\frac{1}{2}} \sum_{n=0}^{\infty} \left(A_n e^{(n + \frac{1}{2})\mu} + B_n e^{-(n + \frac{1}{2})\mu} \right) P_n(\cos \eta) - E_0 z, \tag{B12}$$

where P_n represent Legendre polynomials and the coefficients are represented as

$$A_{n} = \frac{-aE_{0}(2n+1)[e^{(2n+1)\mu_{2}}+1] + V_{1}e^{(2n+1)\mu_{2}} - V_{2}}{e^{(2n+1)U} - 1},$$

$$B_{n} = \frac{aE_{0}(2n+1)[e^{(2n+1)\mu_{1}}+1] + V_{2}e^{(2n+1)\mu_{1}} - V_{1}}{e^{(2n+1)U} - 1},$$
(B13)

and the normal derivative at the surface of Sphere 1 (Jeffery, 1912) is

$$\frac{\partial}{\partial n} = -\frac{1}{a}(\cosh \mu_1 - \cos \eta) \frac{\partial}{\partial \mu},\tag{B14}$$

Thus, (B11) can be deduced into

$$E_{A} = -\left(\frac{\partial V}{\partial n}\right)_{\mu = -\mu_{1}, \eta = \pi}$$

$$= \frac{1}{a}(\cosh \mu_{1} + 1)^{\frac{3}{2}} \sum_{n=0}^{\infty} (2n+1)e^{\left(n+\frac{1}{2}\right)\mu_{1}} A_{n} P_{n}(-1),$$
(B15)

Acknowledgments

This research was supported by the U.S. National Science Foundation under grants AGS-1135446 and AGS-1623780 to The Pennsylvania State University. All data are available at https://doi.org/10.18113/D36W9N.

References

Allen, N. L., & Ghaffar, A. (1995). The conditions required for the propagation of a cathode-directed positive streamer in air. *Journal of Physics D: Applied Physics*, 28, 331–337.

Atlas, D., & Ludlam, F. H. (1961). Multi-wavelength radar reflectivity of hailstorms. Quarterly Journal of the Royal Meteorological Society, 87(374), 523–534. https://doi.org/10.1002/qj.49708737407

Auer, A. H. (1972). Distribution of graupel and hail with size. *Monthly Weather Review*, 100(5), 325–328. https://doi.org/10.1175/1520-0493-100-05-0325

Babich, L., Bochkov, E., Kutsyk, I., Neubert, T., & Chanrion, O. (2016). Positive streamer initiation from raindrops in thundercloud fields. Journal of Geophysical Research: Atmospheres, 121, 6393–6403. https://doi.org/10.1002/2016JD024901

Babich, L., Bochkov, E., & Neubert, T. (2017). The role of charged ice hydrometeors in lightning initiation. *Journal of Atmospheric and Solar-Terrestrial Physics*, 154, 43–46. https://doi.org/10.1016/j.jastp.2016.12.010

Blyth, A. M., Christian, H. J., & Latham, J. (1998). Corona emission thresholds for three types of hydrometeor interaction in thunderclouds. Journal of Geophysical Research, 103(D12), 13,975 – 13,977. https://doi.org/10.1029/97JD02554

Cai, Q., Jánský, J., & Pasko, V. P. (2017). Initiation of positive streamer corona in low thundercloud fields. *Geophysical Research Letters*, 44, 5758–5765. https://doi.org/10.1002/2017GL073107

Cloete, J. H., & van der Merwe, J. (1998). The breakdown electric field between two conducting spheres by the method of images. *IEEE Transactions on Education*, 41(2), 141–145. https://doi.org/10.1109/13.669724

Cooray, V. (2015). On the mimimum length of leader channel and the minimum volume of space charge concentration necessary to initiate lightning flashes in thunderclouds. *Journal of Atmospheric and Solar-Terrestrial Physics, 136*(Part A), 39–45. https://doi.org/10.1016/j.jastp.2015.09.008

Cooray, V., Berg, M., Akyuz, M., Larsson, A., Zitnik, M., & Scuka, V. (1998). Initiation of ground flashes: Some microscopic electrical processes associated with precipitation particles. In *Proceedings of 24th International Conference on Lightning Protection*. Bermingham, UK.

Davis, M. H. (1964). Two charged spherical conductors in a uniform electric field: Forces and field strength. *Journal of Geophysical Research*, 74(28), 6859.

Dubinova, A., Rutjes, C., Ebert, U., Buitink, S., Scholten, O., & Trinh, G. T. N. (2015). Prediction of lightning inception by large ice particles and extensive air showers. *Physical Review Letters*, 115, 015002. https://doi.org/10.1103/PhysRevLett.115.015002

Dwyer, J. R., & Uman, M. A. (2014). The physics of lightning. *Physics Reports*, 534(4), 147–241. https://doi.org/10.1016/j.physrep.2013.09.004 Dye, J., Jones, J., Winn, W., Cerni, T., Gardiner, B., Lamb, D., et al. (1986). Early electrification and precipitation development in a small, isolated Montana cumulonimbus. *Journal of Geophysical Research*, 91(D1), 1231–1247. https://doi.org/10.1029/JD091iD01p01231

Fukao, S., Wakasugi, K., Sato, T., Morimoto, S., Tsuda, T., Hirota, I., et al. (1985). Direct measurement of air and precipitation particle motion by very high-frequency doppler radar. *Nature*, *316*(6030), 712–714. https://doi.org/10.1038/316712a0

ludin, D. I. (2017). Lightning-discharge initiation as a noise-induced kinetic transition. *Radiophysics and Quantum Electronics*, 60(5), 374–394. https://doi.org/10.1007/s11141-017-9807-x

Jackson, J. D. (1999). Classical electrodynamics. New York: John Wiley, Inc.

Jánský, J., & Pasko, V. P. (2017). Modelling of streamer ignition and propagation in the system of two approaching hydrometeors, Abstract AE23B-2492 presented at 2017 AGU Fall Meeting. 11 – 15 Dec.

Jeffery, G. B. (1912). On a form of the solution of Laplace's equation suitable for problems relating to two spheres. *Proceedings of the Royal Society A*, 87(593), 109–120. https://doi.org/10.1098/rspa.1912.0063

Lekner, J. (2011). Near approach of two conducting spheres: Enhancement of external electric field. *Journal of Electrostatics*, 69(6), 559–563. https://doi.org/10.1016/j.elstat.2011.07.009

https://doi.org/10.1016/j.eistat.2011.07.009
Lieberman, M. A., & Lichtenberg, A. J. (2005). *Principles of plasma discharges and materials processing*. New York: John Wiley & Sons, Inc.

Liu, N., Dwyer, J. R., & Rassoul, H. K. (2012). Effects of pressure and humidity on positive corona inception from thundercloud hydrometeors. Journal of Atmospheric and Solar-Terrestrial Physics, 80, 179 – 186. https://doi.org/10.1016/j.jastp.2012.01.012

Liu, N., Kosar, B., Sadighi, S., Dwyer, J. R., & Rassoul, H. K. (2012). Formation of streamer discharges from an isolated ionization column at subbreakdown conditions. *Physical Review Letters*, 109(2), 025002. https://doi.org/10.1016/j.jastp.2015.09.008

Marshall, J. S., & Palmer, W. M. (1948). The distribution of raindrops with size. Journal of the Meteorology, 5(4), 165-166.

Marshall, T. C., Stolzenburg, M., Maggio, C. R., Coleman, L. M., Krehbiel, P. R., Hamlin, T., et al. (2005). Observed electric fields associated with lightning initiation. *Geophysical Research Letters*, 32, L03813. https://doi.org/10.1029/2004GL021802

Mazur, V., Taylor, C. D., & Petersen, D. A. (2015). Simulating electrodeless discharge from a hydrometeor array. *Journal of Geophysical Research: Atmospheres*, 120, 10,879–10,889. https://doi.org/10.1002/2015JD023466

Morrow, R., & Lowke, J. J. (1997). Streamer propagation in air. Journal of Physics D: Applied Physics, 30, 614–627.

Morse, P. M., & Feshbach, H. (1953). Methods of theoretical physics (Vol. 2). New York: McGraw-Hill.

Naidis, G. V. (2005). Conditions for inception of positive corona discharges in air. *Journal of Physics D: Applied Physics*, 38(13), 2211–2214. https://doi.org/10.1088/0022-3727/38/13/020

Nguyen, M. D., & Michnowski, S. (1996). On the initiation of lightning discharge in a cloud 2. The lightning initiation on precipitation particles. *Journal of Geophysical Research*, 101(D21), 26,675–26,680. https://doi.org/10.1029/96JD02338

Proctor, D. E. (1991). Regions where lightning flashes began. *Journal of Geophysical Research*, 96(D3), 5099–5112. https://doi.org/10.1029/90JD02120



Journal of Geophysical Research: Atmospheres

10.1029/2018JD028407

Qin, J., Celestin, S., & Pasko, V. P. (2011). On the inception of streamers from sprite halo events produced by lightning discharges with positive and negative polarity. *Journal of Geophysical Research*, *116*, A06305. https://doi.org/10.1029/2010JA016366 Raizer, Y. P. (1991). *Gas discharge physics*. Berlin: Springer.

 $Rakov, V., \&\, Uman, M.\, (2003). \, \textit{Lightning physics and effects} \,\, (1st\,ed.). \, Cambridge: Cambridge\, University\, Press.$

Sadighi, S., Liu, N., Dwyer, J. R., & Rassoul, H. K. (2015). Streamer formation and branching from model hydrometeors in subbreakdown conditions inside thunderclouds. *Journal of Geophysical Research: Atmospheres, 120,* 3660–3678. https://doi.org/10.1002/2014JD022724

Shi, F., Liu, N., & Rassoul, H. K. (2016). Properties of relatively long streamers initiated from an isolated hydrometeor. *Journal of Geophysical Research: Atmospheres*, 121, 7284–7295. https://doi.org/10.1002/2015JD024580

Stolzenburg, M., Marshall, T. C., Rust, W. D., Bruning, E., MacGorman, D. R., & Hamlin, T. (2007). Electric field values observed near lightning flash initiations. *Geophysical Research Letters*, 34, L04804. https://doi.org/10.1029/2006GL028777

Testud, J., Oury, S., Black, R. A., Amayenc, P., & Dou, X. (2001). The concept of "normalized" distribution to describe raindrop spectra: A tool for cloud physics and cloud remote sensing. *Journal of Applied Meteorology*, 40(6), 1118–1140.

Waldvogel, A. (1974). The N₀ jump of raindrop spectra. *Journal of the Atmospheric Sciences*, 31(4), 1067–1078.

Wisner, C., Myers, C., & Orville, H. D. (1972). A numerical model of a hail-bearing cloud. *Journal of the Atmospheric Sciences*, 29(6), 1160–1181. https://doi.org/10.1175/1520-0469(1972)029<1160:ANMOAH>2.0.CO;2

